Can a galaxy redshift survey measure dark energy clustering?

Masahiro Takada*
Astronomical Institute, Tohoku University, Sendai 980-8578, Japan

A wide-field galaxy redshift survey allows one to probe galaxy clustering at largest spatial scales, which carries invaluable information on horizon-scale physics complementarily to the cosmic microwave background (CMB). Assuming the planned survey consisting of $z \sim 1$ and $z \sim 3$ surveys with areas of 2000 and 300 deg^2, respectively, we study the prospects for probing dark energy clustering from the measured galaxy power spectrum, assuming the dynamical properties of dark energy are specified in terms of the equation of state and the effective sound speed $c_{\rm e}$ in the context of an adiabatic cold dark matter dominated model. The dark energy clustering adds a power to the galaxy power spectrum amplitude at spatial scales greater than the sound horizon, and the enhancement is sensitive to redshift evolution of the net dark energy density, i.e. the equation of state. We find that the galaxy survey, when combined with CMB expected from the Planck satellite mission, can distinguish dark energy clustering from a smooth dark energy model such as the quintessence model ($c_{\rm e} = 1$), when $c_{\rm e} \lesssim 0.04$ (0.02) in the case of the constant equation of state $w_0 = -0.9$ (-0.95). An ultimate full-sky survey of $z \sim 1$ galaxies allows the detection when $c_{\rm e} \lesssim 0.08$ (0.04) for $w_0 = 0.9$ (-0.95). These forecasts show a compatible power with an all-sky CMB and galaxy cross-correlation that probes the integrated Sachs-Wolfe effect. We also investigate a degeneracy between the dark energy clustering and the non-relativistic neutrinos implied from the neutrino oscillation experiments, because the two effects both induce a scale-dependent modification in the galaxy power spectrum shape at largest spatial scales accessible from the galaxy survey. It is shown that a wider redshift coverage can efficiently separate the two effects by utilizing the different redshift dependences, where dark energy clustering is apparent only at low redshifts $z \lesssim 1$.

PACS numbers: 98.65.Dx,98.70.Vc,98.80.Es

I. INTRODUCTION

Various cosmological probes such as supernovae in distant galaxies [1, 2], the cosmic microwave background (CMB) sky [3], and the galaxy redshift surveys [4, 5, 6, 7] have given strong evidence that a dark energy component, such as the cosmological constant, constitutes approximately 70% of the total energy density of the universe, which derives the accelerating cosmic expansion at low redshifts. Because there is no plausible theoretical explanation for its existence and magnitude (e.g. see [8, 9]), observational exploration of the nature of dark energy is one of the most important issues in modern cosmology as well as particle physics.

An observational dark energy task we should first explore to tackle this fundamental problem would be to determine whether the accelerating expansion is as a consequence of the cosmological constant. Relaxing this assumption leads to a generalized dark energy with dynamically evolving energy density, which can be characterized by a time-dependent equation of state $w(a) = p_{\rm de}/\rho_{\rm de}$ (the cosmological constant corresponds to $w = -1$). The current level of accuracy in constraining the constant w-parameter is $\sigma(w) \sim 0.1$ at 1σ level with the best-fit value containing a model with $w = -1$ (e.g. see [3, 7, 10]). Future prospects aimed at pinning down the constraint on w by a factor of 10 have been extensively investigated to address the usefulness of various cosmological experiments based on massive galaxy surveys such as tomographic weak lensing experiment (e.g. [11, 12]), the baryon oscillation experiment (e.g. [13, 14, 15]) and the cluster abundance experiment (e.g. [16]).

Another important consequence of a generalized dark energy is the spatial perturbation, providing an independent clue to resolving the nature of dark energy from the equation of state. There are many previous efforts made to study how an inclusion of the dark energy perturbations modify the cold dark matter (CDM) structure formation scenarios: theoretical predictions on the modifications in the CMB power spectra and the galaxy power spectra [11, 17, 18, 19, 20, 21, 22, 23, 24, 25] and the observational exploration of the dark energy clustering signal from the WMAP data at low multipoles [3, 26, 27, 28]. The dark energy clustering is relevant only for structure formation at low redshifts $z \lesssim 1$, where the net energy density is dominant to the cosmic expansion. In addition, a reasonable model including the dark energy perturbation predicts that the dark energy can cluster together with matter components at large spatial scales (inevitably at super-horizon scales), whilst the dark energy is smooth at small scales so that the additional component does not largely change the small-scale structure formations such as galaxy formation. For these reasons, the dark energy clustering effect on the CMB observables is likely to appear only via the integrated Sachs-Wolfe effect (ISW) at low multipoles, where the Sachs-Wolfe effect generated at the recombination epoch is significant contamination to separate the ISW effect from the measured power spectrum.

*Electronic address: takada@astr.tohoku.ac.jp

The transition scale to divide the dark energy clustering and smooth regimes can be usefully modeled by the effective sound speed of dark energy [22, 29]. In this model, smoothness of dark energy can be tested by searching for the signature of the sound speed from cosmological observables. Hu and Scranton [30] carefully investigated a prospect of how the ISW effect measured via the angular cross-correlation between CMB and galaxy distribution can be used to probe the dark energy clustering, assuming an all-sky, deep multi-color imaging galaxy survey out to $z \sim 2$.

A galaxy redshift survey offers an alternative means for probing the dark energy clustering, through the measured statistical properties of three-dimensional gravitational clustering at largest scales. Compared to the angular correlations, from a cosmological point of view, the redshift survey carries more information on the underlying mass distribution due to a gain of the modes along the line-of-sight or redshift direction. Therefore, the purpose of this paper is to, for the first time, investigate the ability of a galaxy redshift survey for testing the smoothness of dark energy from the measured galaxy power spectrum. In fact, there are several future plans for high-redshift galaxy surveys that are already being constructed or seriously under consideration: the Fiber Multiple Object Spectrograph (FMOS) on Subaru telescope [31], its significantly expanded version, WFMOS [32], the Hobby–Ebery Telescope Dark Energy eXperiment (HETDEX) [33], and the Cosmic Inflation Probe (CIP) mission [34]. These surveys probe galaxies at higher redshifts $z \gtrsim 0.5$ than the existing surveys such as SDSS and 2dF surveys. Such a high-redshift survey has several advantages over the lower redshift ones. First, given a fixed solid angle, the comoving volume in which we can observe galaxies is larger at higher redshifts than in the local universe, thereby reducing the sample variance. This would make it more straightforward to obtain a well-behaved survey geometry that can help measure largest-scale perturbations. Second, density perturbations at smaller spatial scales are still in the linear regime or only in the weakly non-linear regime at higher redshift, which gives us more leverages on measuring the shape of the linear power spectrum to break the parameter degeneracies. In this paper, we will consider the survey design close to the proposed WFMOS survey, which consists two types of surveys different in redshift coverage and survey area: $0.5 \leq z \leq 1.3$ with 2000 degree^2 and $2.5 \leq z \leq 3.5$ with 300 degree^2, respectively. The redshift coverage of WFMOS is suitable to probe the dynamical dark energy whose effects are apparent only at low redshifts $z \lesssim 1$, as we will show below.

The structure of this paper is as follows. In Sec. II we start with writing down background cosmological equations, the Hubble expansion and the angular diameter distance, in terms of cosmological parameters. In Sec. III, we define the effective sound speed parameter to model dynamical properties of dark energy clustering, and review how the dark energy clustering leads to a scale-dependent modification in the linear power spectrum shape assuming the adiabatic initial condition. Sec. IV defines the galaxy power spectrum in terms of the primordial power spectrum, the transfer functions and the scale-dependent growth rate of mass clustering. In Sec. V, we first define survey parameters intended to resemble a future survey being planned, and describe a methodology to model the galaxy power spectrum observed from a redshift survey that includes the two-dimensional nature in the line-of-sight and transverse directions due to the cosmological and redshift distortion effects. We then present the Fisher information matrix formalism that is used to estimate the projected uncertainties in the cosmological parameter determination provided the measured galaxy power spectrum. In Sec. VI we show the prospects of the future survey for probing the dark energy clustering. In addition, we carefully study how a degeneracy between the dark energy clustering and massive neutrinos can be lifted by utilizing the redshift information of galaxy clustering. Finally, we present conclusion and some discussion in Sec. VII.

II. PRELIMINARIES: COSMOLOGY

Throughout this paper, we work in the context of spatially flat CDM models for structure formation (e.g. see [35] and [36]). According to the Einstein general relativity, the expansion history of the universe is given by the scale factor $a(t)$, which is related to redshift via $1 + z = 1/a$ (we use $a(t_0) = 1$ today for our convention). The cosmic expansion during the matter dominated epoch is determined by density contributions from non-relativistic matter $\Omega_{\rm m}$ and dark energy $\Omega_{\rm de}$ at present, in units of the critical density $3H_0^2/8\pi G$, where $H_0 = 100\ h$ km s^{-1}Mpc^{-1} is the Hubble constant. The Hubble expansion rate is given by

$$H^2(a) = H_0^2 \left[\Omega_{\rm m} a^{-3} + \Omega_{\rm de} a^{-3(1+w_0)}\right], \qquad (1)$$

where we have assumed the constant equation of state of dark energy,

$$w_0 \equiv \frac{p_{\rm de}(a)}{\rho_{\rm de}(a)} = -\frac{1}{3}\frac{d\ln\rho_{\rm de}}{d\ln a} - 1 = \text{const.} \qquad (2)$$

Note that $w_0 = -1$ corresponds to the cosmological constant. In this paper we restrict ourselves to a dark energy model with $w_0 \geq -1$ for simplicity.

The comoving angular diameter distance is expressed in terms of the Hubble parameter as

$$D_A(a) = \int_1^a \frac{da}{H^2(a')a'^2}, \qquad (3)$$

giving the distance-redshift relation via $1 + z = 1/a$.

III. DARK ENERGY CLUSTERING FOR ADIABATIC INITIAL CONDITION

To model dark energy clustering, we employ a phenomenological model developed in [22]. In this model, the stress perturbation of dark energy, which governs properties of the dark energy clustering, is usefully specified by the dark energy equation of state and the effective sound speed $c_{\rm e}$, where the latter is needed to model the non-adiabatic stress perturbation (also see [18]). The effective sound speed of a generalized dark energy is defined as

$$c_{\rm e}^2 \equiv \left.\frac{\delta p_{\rm de}}{\delta\rho_{\rm de}}\right|_{\rm rest}, \tag{4}$$

in a "rest frame" coordinate system where the momentum density of the dark energy vanishes. For a more general coordinate system such as Newtonian gauge, the pressure perturbation of dark energy, which enters into the r.h.s. of the momentum conservation equation, can be expressed as

$$\begin{aligned}\delta p_{\rm de} &= w_0\delta\rho_{\rm de} + \bar\rho_{\rm de}(c_{\rm e}^2 - w_0)\left(\delta_{\rm de} + 3\frac{\dot a}{a}\frac{u_{\rm de}}{k}\right)\\ &= c_{\rm e}^2\delta\rho_{\rm de} + 3\frac{\dot a}{a}(c_{\rm e}^2 - w_0)\frac{u_{\rm de}}{k}\bar\rho_{\rm de},\end{aligned} \tag{5}$$

where the first and second terms in the first line on the r.h.s. denote the adiabatic and non-adiabatic pressure perturbations, respectively, $u_{\rm de}$ denotes the peculiar velocity of dark energy, and we have assumed $w_0 =$ constant in time. Note that setting $u_{\rm de} = 0$ in Eq. (5) (corresponding to the rest frame of dark energy perturbations) reduces the pressure perturbation to the form given by Eq. (4). From Eq. (5), one can find that presence of the effective sound speed leads the pressure perturbation to act as a restoring force against the gravitational instability just like the Jeans instability of baryon perturbation (e.g., see Sec. 16 in [42]); in the overdensity ($\delta_{\rm de} > 0$) and underdensity ($\delta_{\rm de} < 0$) regions, the pressure perturbation prevents further collapse and expansion, respectively, if the wavelength of perturbation is smaller than the sound horizon (see below). Conversely, for a model that has only the adiabatic pressure perturbation ($\delta p_{\rm de} = w_0\delta\rho_{\rm de}$), the pressure perturbation and the gravitational force in the momentum conservation equation become $kw_0\delta_{\rm de} + (1+w_0)k\Psi$ (Ψ is the gravitational potential), namely, the two terms have same sign because $w_0 < 0$ and $\Psi \propto -\delta_{\rm de}$ via the Poisson equation: therefore, the pressure perturbation accelerates the gravitational instability on all scales. Note that, throughout this paper, we assume the constant sound speed with $c_{\rm e} \geq 0$ and ignore the trace-free stress perturbation of dark energy for simplicity.

We expect that this modeling to treat the sound speed as a free parameter can cover a broader range of dark energy models rather than working with a specific model of the Lagrangian of dark energy sector. For a scalar field dark energy model, the sound speed can be exactly computed in linear theory in terms of the kinetic energy as a function of the field [19, 28]. For the case of a canonical kinetic energy term such as the quintessence [9, 17, 18, 37], the sound speed $c_{\rm e} = 1$. For a more general modification of the kinetic term such as a phantom energy [38] and a k-essence field [39, 40], a general value of $c_{\rm e}$ including $c_{\rm e} \ll 1$ is allowed.

The dark energy sound speed sets a characteristic length scale in gravitational clustering:

$$\lambda_{\rm de,fs}(a) = \int_0^a da\ \frac{c_{\rm e}}{a^2H(a)}. \tag{6}$$

We shall often call this scale the comoving sound horizon of dark energy at epoch a. One might define the corresponding wavenumber as $k_{\rm de,fs} = 2\pi/\lambda_{\rm de,fs}$. For the scalar-field dark energy model with canonical kinetic energy ($c_{\rm e} = 1$), the sound horizon is comparable with the particle horizon scale. In this paper, we simply refer to a model with $c_e = 1$ as a smooth dark energy model, because a galaxy survey we consider can probe only the galaxy clustering at scales inside the present-day horizon scale and there is no unique definition of smoothness of dark energy on super-horizon scales where the energy density varies depending on the freedom of time-slicing in general relativity.

On large scales $\lambda > \lambda_{\rm de,fs}$, the dark energy perturbation can grow together with non-relativistic matter components. In this case, the gravitational potential Φ in Newtonian gauge[1] evolves in a flat universe (e.g., see [41]) as

$$\Phi(\boldsymbol{k}, a) = \phi_c(a)\mathcal{R}_i(\boldsymbol{k}) \tag{7}$$

where

$$\phi_c(a) \equiv \left(1 - \frac{H(a)}{a}\int_0^a da'\frac{1}{H(a')}\right) \tag{8}$$

and $\mathcal{R}_i(\boldsymbol{k})$ denotes the primordial curvature perturbation of wavenumber $\boldsymbol{k}$. In the matter dominated regime, $H(a) \propto a^{-3/2}$, leading to $\phi_c \to 3/5$. Here we have employed the adiabatic initial condition for dark energy perturbations; the initial conditions of all the components are set by the primordial curvature perturbation. It is worth noting that, for a cosmological constant model ($w_0 = -1$), Eq. (8) can be rewritten as

$$\begin{aligned}1 - \frac{H(a)}{a}\int_0^a\frac{da'}{H(a')} &= 1 - \frac{H(a)}{a}\left[\left.\frac{a'}{H(a')}\right|_0^a\right.\\ &\qquad \left. + \int_0^a da'\frac{a'}{2H^3(a')}\frac{dH^2(a')}{da'}\right]\\ &\propto \frac{H(a)}{a}\int_0^a da'\frac{1}{H^3(a')a'^3},\end{aligned} \tag{9}$$

[1] More precisely, Φ is the curvature perturbation, but related to the potential perturbation via $\Phi = -\Psi$ when the trace-free stress perturbation is negligible, which is valid at redshifts of our interest.

where we have used the partial integral in the first line on the r.h.s., and $dH^2(a)/da = -3H_0^2\Omega_{\rm m0}a^{-4}$ in the second line. The final expression is equivalent to the well-known formula for the growth rate of mass clustering, for example, given by Eq. (10.12) in [42] (also see [43]).

On the other hand, on small spatial scales $\lambda < \lambda_{\rm de,fs}$, the pressure perturbation of dark energy prevents clustering of the dark energy; the dark energy is thus considered as a smooth component in this limit. The redshift dependence of the gravitational perturbation is given by $\Phi \propto g(a)$ via $1+z = 1/a$, and the growth rate $g(a)$ can be computed (e.g. see [12]) by solving the following differential equation with the initial conditions $g(a_{\rm md}) = 1$ and $dg/da(a_{\rm md}) = 0$ in the deeply matter dominated regime $a_{\rm md}$ (e.g., $a_{\rm md} = 10^{-3}$):

$$2\frac{d^2g(a)}{d\ln a^2} + [5 - 3w(a)\Omega_{\rm de}(a)]\frac{dg(a)}{d\ln a} +3[1 - w(a)]\Omega_{\rm de}(a)g(a) = 0, \qquad (10)$$

where the equation of state is generalized so that it is allowed to have a time dependence $w(a)$, and $\Omega_{\rm de}(a)$ is the dark energy density parameter at epoch a, defined as $\Omega_{\rm de}(a) \equiv 8\pi G\rho_{\rm de}(a)/3H^2(a)$. For a cosmological constant model, the solution of Eq. (10) can be given by the integral form of Eq. (8). Note that in the presence of the non-relativistic neutrinos the growth rate is further modified at scales below the neutrino free streaming scale (see [44]), as we shall discuss below.

Hence, introducing the effective sound speed of the dark energy enforces that the stress perturbation leads the dark energy perturbation to be gravitationally stable on small scales so that small-scale structure formations are not largely modified by the additional component compared to the concordance ΛCDM predictions.

IV. SHAPE OF LINEAR GALAXY POWER SPECTRUM

To model the linear power spectrum including the dark energy perturbation, we use the recipe in [22] to compute the transfer function of the potential perturbation $\Phi(k, z)$ assuming the adiabatic initial condition. Given the primordial power spectrum, the power spectrum of the potential perturbation in the matter dominated regime is given by

$$\Delta^2_\Phi(k,z) = T^2_{\rm de}(k,z)\frac{9}{25}\delta^2_{\mathcal R} \times\left(\frac{D_{cb\nu}(k,z)}{a}\right)^2 T^2(k)\left(\frac{k}{k_0}\right)^{-1+n_s+\frac{1}{2}\alpha_s\ln(k/k_0)}, \qquad (11)$$

where the primordial power spectrum, $P_{\mathcal R}(k) \equiv \langle\mathcal{R}_i^2\rangle$, is specified in terms of the primordial curvature perturbation $\delta_{\mathcal R}$, the spectral tilt n_s and the running index α_s, and $T_{\rm de}(k, z)$ is the fitting formula given in [22] to describe the dark energy clustering contribution as explained below. Note that the primordial power spectrum shape is defined at $k_0 = 0.05$ Mpc^{-1}. In Eq. (11), we have imposed that the super-horizon potential perturbation is related to the primordial curvature perturbation as $\Phi(z_{\rm md}) = (3/5)\mathcal{R}_i$ in the matter dominated regime. The growth rate for the total matter (CDM, baryon plus non-relativistic neutrinos) perturbations are computed using the recipe developed in [45] and normalized as $D_{cb\nu}(k, z) \to ag(z)$ at $k \to 0$. It is also noted that, throughout this paper, we employ the transfer function of matter perturbations, $T(k)$, with baryon oscillations *smoothed out* for simplicity (see Sec. IV.B in [44] for the related discussion).

According to the physical processes described in Sec. III, the fitting function $T_{\rm de}(k, z)$ in Eq. (11) is given in terms of the growth rates at scales smaller and larger than the dark energy sound horizon as

$$T_{\rm de}(k,z) = \frac{1+q^2}{3g(z)/[5\phi_c(z)] + q^2}, \qquad (12)$$

where the variable q is defined as

$$q \equiv \frac{k}{2\pi}\sqrt{\lambda_{\rm de,fs}(z)\lambda_{\rm de,fs}(z_{\rm de})}, \qquad (13)$$

with the redshift $z_{\rm de}$ being given by

$$\frac{\rho_{\rm de}(z_{\rm de})}{\rho_{\rm m}(z_{\rm de})} = \frac{1}{\pi}, \qquad 1 + z_{\rm de} = \left(\pi\frac{\Omega_{\rm de}}{\Omega_{\rm m}}\right)^{-\frac{1}{3w_0}}. \qquad (14)$$

Note that $T_{\rm de} \to 5\phi_c(z)/[3g(z)]$ or 1 as $k \to 0$ or ∞, respectively, which reproduce the two asymptotic regimes discussed in Sec. III. For the cosmological constant model ($w_0 = -1$), $T_{\rm de}(k, z) = 1$ because $3g(z)/[5\phi_c] = 1$ as explained around Eqs. (9) and (10).

Galaxies are biased tracers of the underlying gravitational field. Hence, the linear power spectrum of galaxy distribution is related to the potential power spectrum via the Poisson equation as

$$\frac{k^3P_g(k,z)}{2\pi^2} = b_1^2\left(\frac{2k^2a}{3H_0^2\Omega_{\rm m}}\right)^2\Delta^2_\Phi(k,z) \qquad (15)$$

where b_1 is a scale-independent, linear bias parameter we assume.

As carefully investigated in [22] (see Appendix A of that paper), the fitting formula (12) holds with batter than $\sim 10\%$ accuracy compared to the results obtained by directly solving the multi-fluid Boltzmann equations, for a range of the dark energy parameters we are interested in. In the presence of non-relativistic neutrinos, however, it remains unclear how our treatment of Eq. (11) holds accurate. Hence, an interesting issue is to develop an accurate transfer function for the total matter perturbations including the dark energy as well as neutrino perturbations. This will be our future study and presented elsewhere. For our purpose, which is to *estimate* the ability of future surveys to probe dark energy clustering, our treatment of the galaxy power spectrum

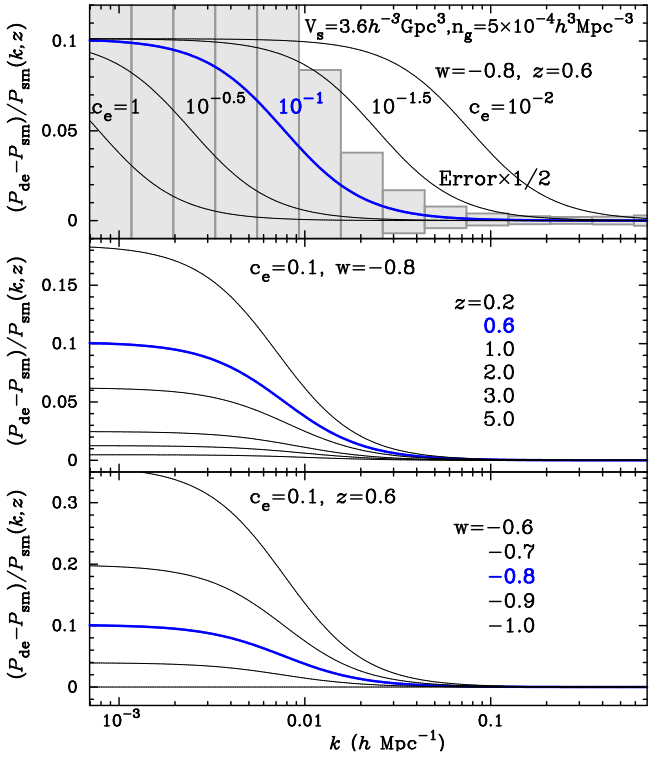

FIG. 1: *Upper panel*: Shown is how the dark energy clustering amplifies the power of linear power spectrum $P(k)$ at $z = 0.6$ on spatial scales greater than the dark energy sound horizon, relative to the smooth dark energy model ($P_{\rm sm}$). Note that non-relativistic neutrinos are ignored in this plot. The dark energy equation of state is taken to $w_0 = -0.8$, and the sound speed is varied to show how the scale-dependent modification in $P(k)$ changes with $c_{\rm e}$: with decreasing $c_{\rm e}$, the transition in $P(k)$ amplitude appears at smaller length scales, i.e. larger k. Shaded boxes around the curve of $c_e = 0.1$ show the expected 1-σ measurement errors for spherically averaged $P(k)$ at each k bin for a survey covering 2000 deg^2 and $0.5 < z < 1.3$ (see text for the details), but note that we have multiplied the error bars by a factor 1/2 for illustrative purpose. Comparing the solid curves with the error bars leads to a naive expectation that the dark energy clustering can be detected from this type of galaxy survey only when the sound speed is smaller than $c_{\rm e} \sim 0.1$. *Middle panel*: Redshift dependence of the power spectrum shape modification due to the dark energy clustering, where $c_{\rm e} = 0.1$ and $w_0 = -0.8$ are fixed. *Lower panel*: As the fiducial value of w_0 is away from $w_0 = -1$, the amplification in $P(k)$ at small k is more enhanced, for a fixed $c_{\rm e} = 0.1$. In all the panels, the bold solid curve shows the same result for $c_e = 0.1$, $w_0 = -0.8$ and $z = 0.6$.

is accurate enough. This is partly justified by the fact that the following results are not largely changed with and without non-relativistic neutrinos, as will be explicitly shown below.

The top panel of Fig. 1 illustrates how the dark energy clustering induces a scale-dependent modification in the shape of linear power spectrum, $P(k)$, at $z = 0.6$, compared to the smooth dark energy model. The dark energy equation of state is fixed to $w_0 = -0.8$, and the fiducial value of the sound speed $c_{\rm e}$ is varied from $c_{\rm e} = 1$ to $c_{\rm e} = 10^{-2}$. Note that $c_{\rm e} = 1$ roughly corresponds to the smooth dark energy model such as the quintessence model, since the sound horizon is comparable with the Hubble horizon. It is clearly seen that, on spatial scales larger than the dark energy sound horizon given by Eq. (6), the dark energy can cluster together with dark matter and thus enhances the power spectrum amplitude compared to the small-scale amplitude that matches the smooth model prediction ($P/P_{\rm sm} = 1$). The transition in $P(k)$ amplitude appears from larger k with decreasing the sound speed c_e, because the dark energy sound horizon gets shorter. It is worth noting that, since we have normalized the primordial power spectrum (see Sec. IV), all the power spectra match at $k \ll k_{\rm de,fs}$ or $k \gg k_{\rm de,fs}$, showing that the effect of dark energy perturbation becomes independent of k. Hence, one can measure $c_{\rm e}$ only if the characteristic transition pattern in the power spectrum shape is accurately measured from observations. In other words, the power spectrum amplitude is not useful to constrain $c_{\rm e}$.

The shaded boxes around the curve of $c_{\rm e} = 0.1$ represent the 1-σ measurement errors on $P(k)$, reduced by a factor 2 for illustrative purpose, for the fiducial galaxy survey with redshift range of $0.5 \le z \le 1.3$ and survey area of 2000 deg^2 corresponding to the comoving volume of $3.6h^{-3}$Gpc^3. Note that the errors are for the power spectrum spherically averaged over angle. It is apparent that the future survey of our interest allows a precise measurement of the linear power spectrum shape, achieving a few % accuracies in each k-bin at $k \gtrsim 0.05h$ Mpc^{-1}, while the errors are dominated by the sample variance at smaller k. A quick look at this plot leads to a naive expectation that, only if the sound speed is sufficiently small such as $c_{\rm e} \lesssim 0.1$, one could measure the transition pattern in $P(k)$ from the galaxy survey. In the following, we shall carefully study how well a future galaxy survey can probe the dark energy clustering fully taking into account degeneracies between cosmological parameters.

In the middle panel we show that the dark energy perturbation more amplifies the power spectrum amplitude at the large spatial scales as one goes to a lower redshift, because the net dark energy density is more prominent at lower redshifts. Observationally this means that a galaxy survey of lower redshift $z \lesssim 1$ is more suitable for exploiting the dark energy perturbations than high-z ones.

Finally, the lower panel of Fig. 1 shows how the effect of dark energy perturbation varies with the fiducial value of the equation of state w_0. With increasing w_0 from $w_0 = -1$, the dark energy perturbation more enhances the amplitude of $P(k)$ at the large scales, because the dark energy density keeps prominent at higher redshift.

Survey	$z_{\rm center}$	$k_{\rm max}$ (hMpc^{-1})	$\Omega_{\rm survey}$ (deg^2)	$V_{\rm s}$ (h^{-3}Gpc^3)	$\bar{n}_{\rm g}$ (10^{-3} h^3Mpc^{-3})	Bias
Gz1 ($0.5 < z < 1.3$)	0.6	0.15	2000	0.57	0.5	1.25
	0.8	0.17	2000	0.81	0.5	1.40
	1.0	0.19	2000	1.0	0.5	1.55
	1.2	0.21	2000	1.2	0.5	1.7
Gz3 ($2.5 < z < 3.5$)	3.0	0.53	300	1.2	1.0	3.3

TABLE I: Galaxy survey specifications that we assume in this paper. We consider two types of galaxy surveys, named as "Gz1" and "Gz3", intended to resemble the WFMOS fiducial survey [32]. The former sees galaxies at $z \sim 1$ with a fixed sky coverage of 2000 deg^2, while the latter probes $z \sim 3$ galaxies with 300 deg^2. $V_{\rm s}$ and $\bar{n}_{\rm g}$ are the comoving survey volume and the comoving number density of sampled galaxies for each redshift slice, respectively. Note that $V_{\rm s}$ is computed for our fiducial cosmological model with $\Omega_{\rm m} = 0.27$, $\Omega_{\rm de} = 0.73$ and $w_0 = -0.8$. $z_{\rm center}$ denotes the centering redshift of each redshift slice, and $k_{\rm max}$ is the maximum wavenumber below which information in the linear power spectrum can be extracted. (We do not use any information above $k_{\rm max}$ in the Fisher information matrix analysis.) "Bias" denotes the assumed linear bias parameters of sampled galaxies.

V. METHODOLOGY

A. Survey Parameters

To derive a realistic parameter forecast, we employ the galaxy survey parameters that are chosen to resemble the future surveys that are under serious consideration. As shown below (see Eq. [18]), the statistical error of the galaxy power spectrum measurement is limited by the survey volume, $V_{\rm s}$, as well as the mean number density of galaxies, $\bar{n}_g$. There are two advantages for a higher redshift survey over the current surveys probing the universe at $z \lesssim 0.3$. First, given a fixed solid angle, the comoving volume in which we can observe galaxies is larger at higher redshifts than in the local universe, thereby reducing the sample variance. In addition, it would be relatively straightforward to obtain a well-behaved survey geometry, e.g., a cubic geometry that would be helpful to probe a largest-scale galaxy clustering as well as handle the systematics under control. Second, density fluctuations at smaller spatial scales are still in the linear regime or only in the weakly non-linear regime at higher redshift, which gives us more leverages on measuring the shape of the linear power spectrum.

We employ the survey parameters that match the fiducial survey design of WFMOS [32], consisting of two types of redshift surveys different in redshift coverage and survey area:

- Gz1: $0.5 < z < 1.3$ and $\Omega_{\rm s} = 2000$ deg^2
- Gz3: $2.5 < z < 3.5$ and $\Omega_{\rm s} = 300$ deg^2

where the names Gz1 and Gz3 stand for the "Ground"-based galaxy surveys probing the universe at $z \sim 1$ and $z \sim 3$, respectively.

Because we have limited knowledge of how galaxies have formed within the CDM hierarchical clustering scenario, it is of critical importance to figure out an optimal survey strategy of which type of galaxies (emission lines) are targeted to achieve the desired scientific goals, given the spectrograph specifications (sensitivity, the number of fibers, wavelength coverage, etc.) and the number of nights allocated. It was shown in [13] (also see [46]) that a survey having $\bar{n}_{\rm g} P_{\rm g} \gtrsim 3$ over the range of wavenumbers considered is close to an optimal design from a cosmological, not practical, point of view, and the hypothetical WFMOS survey parameters were defined in this regard. In this paper, we simply adopt the survey parameters used in [13], which are summarized in Table I.

B. A Galaxy Power Spectrum in Redshift Space

We employ the method developed in [13] (also see [44]) to model a galaxy power spectrum observable from a redshift survey. The power spectrum measures how clustering strength of galaxy distribution varies as a function of 3-dimensional wavenumber, k (or the inverse of 3-dimensional length scale). However, we cannot know a true position of a galaxy in real space from the observables, angular position and redshift. Rather, we have to assume a fiducial cosmology to convert the observed angular position and redshift of galaxies into positions in 3-dimensional space. Since this fiducial cosmology generally differs from the true cosmology, we could introduce distortion in the inferred distribution of galaxies. This cosmological distortion effect is the so-called Alcock-Paczynski (AP) effect [47]. Taking into account the effects of the cosmological distortion, linear redshift distortion [48] and galaxy bias, the galaxy power spectrum in the linear regime can be expressed in terms of the real-space galaxy power spectrum $P_g(k,z)$ (see Eq. [15]) as

$$P_s(k_{\rm fid\perp}, k_{\rm fid\parallel}) = \frac{D_A(z)^2_{\rm fid} H(z)}{D_A(z)^2 H(z)_{\rm fid}} \left[1 + \beta \frac{k_\parallel^2}{k_\perp^2 + k_\parallel^2}\right]^2 \times P_g(k,z), \quad (16)$$

with

$$k_\perp = \frac{D_A(z)_{\rm fid}}{D_A(z)} k_{{\rm fid}\perp}, \qquad k_\parallel = \frac{H(z)}{H_{\rm fid}(z)} k_{{\rm fid}\parallel}, \qquad (17)$$

where $k = (k_\perp^2 + k_\parallel^2)^{1/2}$, $k_\parallel$ and $k_\perp$ denote the components of the wavenumber parallel and perpendicular to the line-of-sight direction, respectively, and β denotes the linear redshift space distortion taking into account the non-relativistic neutrino effect (see [44]), defined as $\beta = -(1/b_1) d\ln D_{{\rm cb}\nu}(k,z)/d\ln(1+z)$. $D_A(z)$ and $H(z)$ are the comoving angular diameter distance and Hubble parameter, respectively, and the quantities with subscript 'fid' denote the quantities in the fiducial cosmological model. Note that $P_g(k,z)$ depends on the scale-independent, linear bias parameter b_1 as $P_g \propto b_1^2$ (see Eq. [15]).

The redshift and cosmological distortion effects are extremely powerful for constraining cosmological parameters. Because the structure formation scenario predicts that the power spectrum $P(k)$ has characteristic features such as the broad peak from the matter-radiation equality, scale-dependent suppression of power due to baryons and non-relativistic neutrinos, the tilt and running of the primordial power spectrum, and the baryonic acoustic oscillations, the distortion effects can be precisely measured with future galaxy surveys from the distorted features and help break degeneracies between parameter determination quite efficiently. There are notably two examples for the prospects. First, the baryon oscillation peaks in $P(k)$ can be used as a standard ruler, allowing precise measurements of $H(z)$ and $D_A(z)$ to constrain the equation of state of dark energy [13, 14, 15, 46]. Second, measuring the redshift distortion helps break strong degeneracy between the power spectrum amplitude and the galaxy bias, allowing a precise determination of the neutrino mass [44].

C. Fisher Matrix Analysis

In order to investigate how well one can constrain the cosmological parameters for a given redshift survey, one needs to specify measurement uncertainties of the galaxy power spectrum. When non-linearity is weak, it is reasonable to assume that observed density perturbations obey Gaussian statistics. In this case, there are two sources of statistical errors on a power spectrum measurement: the sampling variance (due to the limited number of independent wavenumbers sampled from a finite survey volume) and the shot noise (due to the imperfect sampling of fluctuations by the finite number of galaxies). To be more specific, the statistical error on measurement of $P(k)$ at a given wavenumber bin k_i is given in [49] by

$$\left[\frac{\Delta P_s(k_i)}{P_s(k_i)}\right]^2 = \frac{2(2\pi)^2}{V_{\rm s} k^2 \Delta k \Delta\mu}\left[1 + \frac{1}{\bar{n}_g P_s(k_i)}\right]^2, \qquad (18)$$

where $\bar{n}_g$ is the mean number density of galaxies, $V_{\rm s}$ is the comoving survey volume, and μ is the cosine of the angle between $\boldsymbol{k}$ and the line-of-sight direction. Note that we have assumed that the galaxy selection function is uniform over the redshift slice we consider and ignored any boundary effects of survey geometry for simplicity.

The first term in the bracket on the r.h.s of Eq. (18) represents sampling variance. Errors become independent of the number density of galaxies when sampling variance dominates (i.e., $P_s \gg \bar{n}_g$ over the range of k considered), and thus the only way to reduce the errors is to survey a larger volume. On the other hand, the second term represents shot noise, which comes from discreteness of galaxy samples. When shot noise dominates ($P_s \ll \bar{n}_g$), the most effective way to reduce noise is to increase the number density of galaxies by increasing exposure time per field. Note that for a fixed $\bar{n}_g$ the relative importance of shot noise contribution can be suppressed by using galaxies with larger bias parameters, b_1, as $P_s \propto b_1^2$.

We use the Fisher information matrix formalism to convert the errors on $P_s(k)$ into error estimates of model parameters [13, 50]. The Fisher matrix is computed from

$$F_{\alpha\beta} = \frac{V_{\rm s}}{8\pi^2}\int_{-1}^{1} d\mu \int_{k_{\rm min}}^{k_{\rm max}} k^2 dk \, \frac{\partial \ln P_s(k,\mu)}{\partial p_\alpha}\frac{\partial \ln P_s(k,\mu)}{\partial p_\beta} \times \left[\frac{\bar{n}_g P_s(k,\mu)}{\bar{n}_g P_s(k,\mu)+1}\right]^2, \qquad (19)$$

where p_α expresses a set of parameters. The partial derivative with respect to a given parameter p_α is evaluated around the fiducial model. When combined with the CMB constraints, we simply add the CMB and galaxy fisher matrices, $F_{\mu\nu} = F^g_{\mu\nu} + F^{\rm CMB}_{\mu\nu}$, to obtain the joint constraints. The 1σ error on p_α marginalized over the other parameters is given by $\sigma^2(p_\alpha) = (\boldsymbol{F}^{-1})_{\alpha\alpha}$, where $\boldsymbol{F}^{-1}$ is the inverse of the Fisher matrix. We follow the method described in [12] when we consider projected constraints in a two-parameter subspace to see how the two parameters are correlated.

To calculate $F_{\alpha\beta}$ in Eq. (19), we need to specify $k_{\rm min}$ and $k_{\rm max}$ for a given galaxy survey. We use the upper limit, $k_{\rm max}$, to exclude information in the non-linear regime, where the linear theory prediction of density fluctuations, Eq. (16), becomes invalid. Following [13], we adopt the values of $k_{\rm max}$ for each redshift slices as given in Table I. As for the minimum wavenumber, we use $k_{\rm min} = 10^{-5}$ Mpc^{-1}, which gives well-converged results for all the cases we consider.

D. Model Parameters of a CDM Model

The Fisher matrix formalism assesses how well given observables can distinguish the true ("fiducial") cosmological model from other models. The parameter forecasts we obtain depend on the fiducial model and are also sensitive to the choice of free parameters. We include a fairly broad range of the CDM dominated cosmology: the density parameters are $\Omega_{\rm m}(=0.27)$, $\Omega_{\rm m}h^2(=0.14)$,

and $\Omega_{\rm b}h^2(=0.024)$ (note that we assume a flat universe); the primordial power spectrum parameters are the spectral tilt, $n_s(=1)$, the running index, $\alpha_s(=0)$, and the normalization parameter of primordial curvature perturbation, $\delta_{\mathcal{R}}(=5.07\times10^{-5})$ (the values in the parentheses denote the fiducial model). The linear bias parameters, b_1, are included for each redshift slice as given in Table I.

The dark energy parameters, the equation of parameter w_0 and the sound speed $c_{\rm e}$, are allowed to vary in order to study how the constraint on $c_{\rm e}$ changes with the assumed fiducial values. We also include the non-relativistic neutrinos as free parameters (see [44] for the details). The neutrino oscillation experiments have provided strong evidence that two or three of standard three-flavor neutrinos have finite mass (e.g. see [51] for a review). We assume throughout this paper that some of the three species are massive and have become non-relativistic until the present. The non-relativistic neutrinos affect the structure formation by suppressing the growth of matter density fluctuations at small spatial scales owing to their large velocity dispersion. Hence, the non-relativistic neutrinos induce a scale-dependent modification in the power spectrum shape. For a range of the total neutrino mass implied from the neutrino oscillation experiments, the effects of non-relativistic neutrinos and dark energy clustering could be degenerate in a galaxy power spectrum, especially when the dark energy sound horizon is comparable with the neutrino free-streaming scale. We shall below study this issue quantitatively. The neutrino parameters we assume are the ratio of the total neutrino mass density, $f_\nu(\equiv\Omega_\nu/\Omega_{\rm m}=0.01)$, corresponding to the total neutrino mass 0.13 eV, and the number of non-relativistic neutrino species, $N_\nu^{\rm nr}(=2)$. The fiducial values of f_ν and $N_\nu^{\rm nr}$ are consistent with the neutrino oscillation experiment results (see Fig. 3 in [44]) as well as the upper bounds set from the cosmological experiments [3, 4, 52]. In summary, for a survey which consists of N_s redshift slices, we have $10+N_s$ parameters in total:

$$p_\alpha = \{\Omega_{\rm m}, \Omega_{\rm m}h^2, \Omega_{\rm b}h^2, \delta_{\mathcal{R}}, n_s, \alpha_s, w_0, c_{\rm e}, f_\nu, N_\nu^{\rm nr}, b_1(z_1), \cdots, b_1(z_{N_s})\}\,. \quad (20)$$

As shown in the literature (e.g., see [3]), a galaxy survey alone cannot determine all the cosmological parameters simultaneously, but would leave some parameter combinations degenerated. Combining the galaxy survey constraints with the constraints from CMB temperature and polarization anisotropies can be a powerful way to lift parameter degeneracies [53]. When computing the Fisher matrix of CMB, we employ 7 parameters: 6 parameters (the parameters above minus the dark energy, neutrino and bias parameters) plus the Thomson scattering optical depth to the last scattering surface, $\tau(=0.10)$. Note that our treatment is rather conservative: we do not use any CMB constraints on the dark energy parameters and the non-relativistic neutrinos. The Fisher matrix for the joint experiment is given by adding the CMB Fisher matrix to the galaxy Fisher matrix as $F_{\alpha\beta}=F^{\rm g}_{\alpha\beta}+F^{\rm CMB}_{\alpha\beta}$. We entirely ignore the contribution to the CMB from the primordial gravitational waves. We use the publicly-available CMBFAST code [54] to compute the angular power spectra of temperature anisotropy, $C_l^{\rm TT}$, E-mode polarization, $C_l^{\rm EE}$, and their cross correlation, $C_l^{\rm TE}$. Specifically we consider the noise per pixel and the angular resolution of the Planck experiment that were assumed in [53]. Note that we use the CMB information in the range of multipole $10\le l\le 2000$, and therefore we do not include the ISW effect at low multipoles $l\lesssim 10$ which the dark energy perturbation may affect.

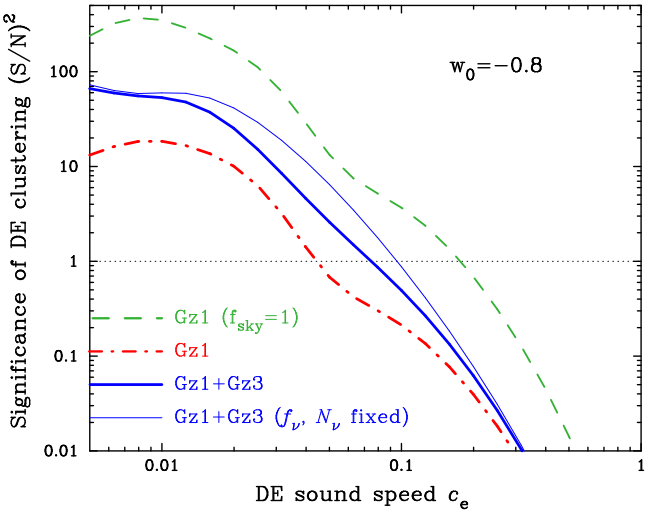

FIG. 2: A significance of discriminating the dark energy clustering model from a smooth dark energy model ($c_e=1$) as a function of the fiducial value of $c_{\rm e}$, expected from the galaxy survey combined with Planck. The fiducial value of the dark energy equation of state is kept fixed to $w_0=-0.8$. The bold solid curve shows the forecast for the nominal survey design of WFMOS (see Table I), while the dot-dashed curve shows the result when the Gz1 survey alone is used. The dashed curve shows the result for an ultimate all-sky survey of $z\sim1$ galaxies.

VI. RESULTS

A. Forecasts for Testing Dark Energy Clustering

As can be seen from Fig. 1, the effect of dark energy clustering on the linear power spectrum is only apparent for variations that span an order of magnitude in $c_{\rm e}$ (also see [30] for the similar discussion). We therefore use

$$p_{c_{\rm e}} = \log_{10} c_{\rm e}, \quad (21)$$

as a free parameter in the Fisher matrix calculation rather than directly using c_e. Then, we define the following quantity to estimate the significance of how well the future galaxy survey we consider can discriminate between a given $c_{\rm e}$ model and a smooth dark energy model

with $c_{\rm e} = 1$:

$$\left(\frac{S}{N}\right)^2\Big|_{c_{\rm e}} = \left(\frac{\log_{10} c_{\rm e}}{\sigma(\log_{10} c_{\rm e})}\right)^2, \qquad (22)$$

where $\sigma(\log_{10} c_{\rm e}) \equiv \sqrt{(\boldsymbol{F}^{-1})_{p_{c_{\rm e}} p_{c_{\rm e}}}}$, the 68% C.L. error on $p_{c_{\rm e}}$ marginalized over the other parameter uncertainties.

The bold solid curve in Fig. 2 shows the forecasted significance $(S/N)^2$ to discriminate between a dark energy clustering model and the smooth model, for the WFMOS fiducial survey (Gz1 plus Gz3 in Table I) combined with Planck. Note that the fiducial value of $w_0 = -0.8$ is assumed here. It is clearly seen that the dark energy clustering can be distinguished at significance $(S/N) \gtrsim 1$ as the fiducial value of $c_{\rm e}$ gets smaller than $c_{\rm e} \approx 0.08$, where the dark energy sound horizon scale enters into a window of the wavenumbers where the galaxy power spectrum can be precisely measured with the galaxy survey (see Fig. 1). However, for too low sound speeds such as $c_{\rm e} \lesssim 0.01$, S/N saturates at $c_{\rm e} \lesssim 0.01$ (or the dashed and dot-dashed curves even have a peak around $c_{\rm e} \sim 0.01$). This is because the transitions in $P_g(k, z)$ occur at k comparable with or larger than the maximum wavenumber $k_{\rm max}$ above which the linear power spectrum information is not available due to the non-linearities in structure formation. On the other hand, the significance drops off rapidly as $c_{\rm e} \to 1$ because the transitions occur at too large spatial scales where the galaxy power spectrum measurement is largely limited by the sample variance. One may also notice that the curves appear to have a jagged feature around $c_{\rm e} = 0.05$. This arises from degeneracies between dark energy clustering and non-relativistic neutrinos. This can be partly seen from the thin solid curve, which shows the results when the neutrino parameters f_ν and $N_\nu^{\rm nr}$ are fixed to the fiducial values; the jagged feature disappears. We shall come back to this issue below in more detail.

The dot-dashed curve shows the result when the Gz1 survey alone is combined with Planck. Comparing the solid and dot-dashed curves clarifies that the constraint on dark energy clustering is mainly from the lower redshift survey compared to the $z \sim 3$ survey, because the net dark energy density is more prominent at lower redshifts (see Fig. 1). The dashed curve shows the forecast for an ultimate full-sky redshift survey of $z \sim 1$, hypothetically obtained by enlarging the survey area of $z \sim 1$ by a factor of 20. In this case, the model with $c_{\rm e} \lesssim 0.2$ can be detected at more than a 1-σ level. This result might be compared with Fig. 8 in [30]; the authors investigated the ISW effect to probe dark energy clustering via the CMB-galaxy cross-correlation measurements assuming a full-sky CMB map and a full-sky, multi-color galaxy imaging survey out to $z \sim 2$. Interestingly, our results show a similar-level precision of constraining dark energy clustering to theirs, although our method does not include the CMB information on dark energy clustering (see Sec. V D), and the survey area ($f_{\rm sky} \sim 0.05$) and the redshift range are much smaller and narrower than theirs,

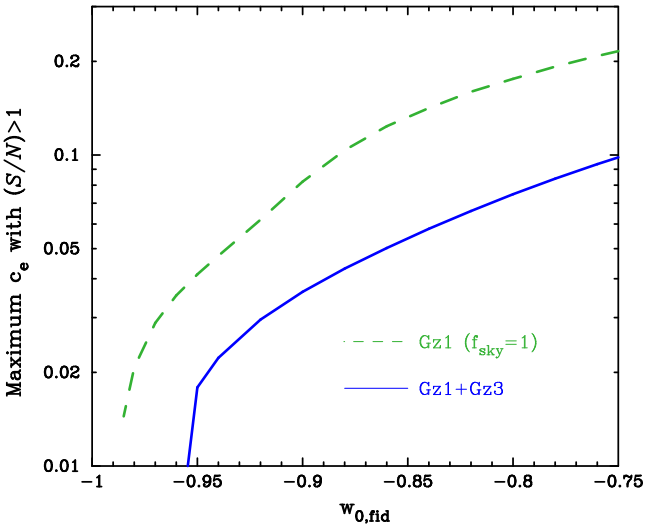

FIG. 3: A maximum dark energy sound speed with $(S/N)|_{c_{\rm e}} \geq 1$ against the fiducial value of w_0. The solid and dashed curves are the results for WFMOS (Gz1 plus Gz3) and the full-sky $z \sim 1$ survey, respectively. As the underlying true cosmology approaches to the cosmological constant model, one can detect dark energy clustering from a galaxy survey only when the sound speed $c_{\rm e}$ is sufficiently small.

respectively. This would be partly because a galaxy power spectrum contains more independent modes of linear fluctuations in the line-of-sight direction compared to the angular correlations. It is also noticed that comparing the dashed curve with the dot-dashed (or solid) curve shows about factor 20 increase in $(S/N)^2$, corresponding to the gain in the sky coverage $f_{\rm sky}$. This implies that the constraint on $c_{\rm e}$ is mainly from the galaxy survey, not as a result of breaking the parameter degeneracies obtained by combining the galaxy survey with CMB, as expected. In summary, we conclude from the results in Fig. 2 that a wide-field galaxy redshift survey by its own offers an alternative, vital opportunity for testing the smoothness of dark energy.

Obviously, the ability to detect dark energy clustering from a galaxy survey depends upon the net dark energy density or equivalently upon the equation of state w_0 in our setting for a fixed $c_{\rm e}$, provided $\Omega_{\rm de}$ and $\Omega_{\rm m}$ are tightly constrained. Fig. 3 shows a maximum sound speed detectable with $(S/N) \geq 1$ as a function of the given fiducial value of w_0. As dark energy becomes close to the cosmological constant ($w_0 = -1$), it is getting more difficult to detect dark energy clustering: dark energy clustering can be discriminated only if the sound speed is sufficiently small so that the scale-dependent transitions in $P_g(k)$ are measurable to within the measurement accuracies. To be more specific, the model with $w_0 \gtrsim -0.96$ allows a test of the dark energy smoothness for the WFMOS survey, while the model with $w_0 \gtrsim -0.98$ can be tested for the ultimate full-sky survey. Alternatively, if the true cosmology has $w_0 = -0.9$ (-0.95), the dark energy clustering can be detected when $c_{\rm e} \lesssim 0.02$ (0.04), while the full-sky

survey allows the detection when $c_{\rm e} \lesssim 0.04$ (0.08), a factor of 2 improvement over WFMOS.

B. Parameter Degeneracies

To more quantitatively understand the forecast for constraining the dark energy clustering shown in the preceding subsection, it is useful to examine how the parameters are degenerate with each other given the survey data sets. Table II gives the correlation coefficients between the dark energy sound speed and the other parameters for the WFMOS survey (Gz1 plus Gz3) combined with Planck. In the context of the Fisher information matrix formalism, the correlation coefficient is defined as

$$r \equiv \frac{(\boldsymbol{F}^{-1})_{p_{c_{\rm e}} p_\alpha}}{\sqrt{(\boldsymbol{F}^{-1})_{p_{c_{\rm e}} p_{c_{\rm e}}} (\boldsymbol{F}^{-1})_{p_\alpha p_\alpha}}}, \tag{23}$$

where p_α denotes one of the model parameters. When the coefficient $|r| = 1$, the two parameters are totally degenerate, while $r = 0$ means they are uncorrelated. While the coefficients varies with the fiducial model, we have assumed $w_0 = -0.8$ and $c_{\rm e} = 0.05$ for the fiducial values of the dark energy parameters, where $c_{\rm e} = 0.05$ roughly corresponds to the dip scale of the curves in Fig. 2 (also see below for a more detailed discussion). Table II shows that the dark energy sound speed is most degenerate with the non-relativistic neutrino parameter $N_\nu^{\rm nr}$ as expected, because a change in $N_\nu^{\rm nr}$ affects the shape of linear power spectrum via the change in the neutrino free-streaming scale[2], but is insensitive to the $P(k)$ amplitude; the suppression rate in $P(k)$ amplitude due to the neutrino free-streaming is primarily sensitive to another neutrino parameter f_ν as $\Delta P(k)/P(k) \approx -8 f_\nu$ in the small-scale limit (see Fig. 2 in [44]). On the other hand, the sound speed is only weakly correlated with the other parameters. Encouragingly, therefore, while the parameters, $\Omega_{\rm m}h^2, \Omega_{\rm b}h^2, n_s$ and α_s, also modify the shape of power spectrum, combining the galaxy survey with Planck is a very powerful way to efficiently lift the parameter degeneracies (also see [44] for the extensive discussion on the degeneracies between the neutrino parameters and the primordial spectrum shape parameters).

It is also worth noting that the sound speed is only weakly correlated with the parameters controlling the galaxy power spectrum amplitude such as $\delta_{\mathcal{R}}$ and b_1, again verifying that the constraint on $c_{\rm e}$ is primarily from the shape of galaxy poser spectrum rather than the amplitude information. Our method given in Sec. V B includes the redshift distortion effect on the galaxy power spectrum, which significantly helps break the degeneracy between the power spectrum amplitude and the galaxy bias. We have checked that ignoring the redshift distortion effect little changes our results. Hence, constraining $c_{\rm e}$ with the galaxy survey, if detected, is generally robust against uncertainties involved in galaxy bias.

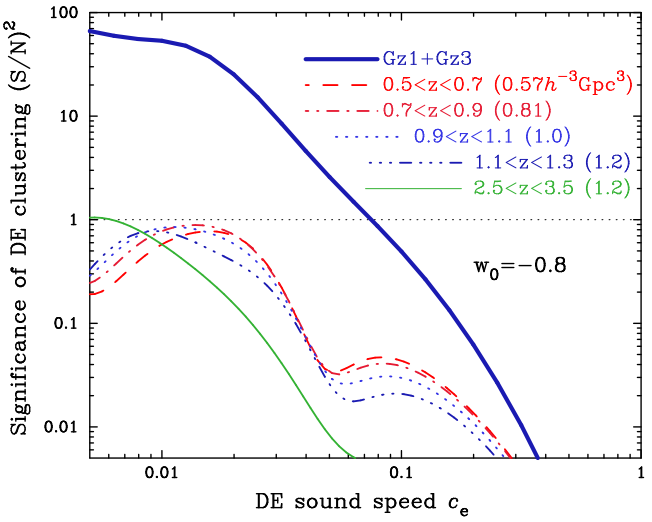

FIG. 4: Shown is how each redshift slice of the WFMOS survey contributes to the dark energy constraint shown in Fig. 2. The number in the parenthesis for the label of each curve denotes the comoving survey volume for each redshift slice (see Table I). The lowest redshift slice ($0.5 \le z \le 0.7$) yields most contribution even though the slice has the smallest survey volume and the smallest $k_{\rm max}$, as dark energy is more prominent at lower redshifts. Also interesting is a jagged feature appears around $c_{\rm e} \approx 0.05$ when one redshift slice alone is used, while the jagged feature is significantly weakened when all the slices are combined. The reasons for this to happen are explained in text as well as the subsequent figures.

C. Dark Energy Clustering and Massive Neutrinos

In this subsection, we investigate in more detail the degeneracies between the dark energy sound speed and the non-relativistic neutrinos.

In Fig. 4 we start with looking into the significance $(S/N)^2$, as in Fig. 2, but for the case when only one of the redshift slices listed in Table I is used. All the curves for each slice of Gz1 show a more prominent jagged feature around $c_{\rm e} = 0.05$ than the solid curve for all the slices combined, implying that the constraint on $c_{\rm e}$ is weakened due to the parameter degeneracies, because the dark energy sound horizon becomes comparable with the neutrino free-streaming scale for a redshift range accessible from the galaxy survey (we shall show this more explicitly below). However, most important result shown here is the parameter degeneracies can be quite efficiently broken, when all the redshift slices are combined, as shown by the bold solid curve. This implies that a survey with wider redshift coverage can efficiently separate the two effects from the measured $P(k)$.

[2] Note that the neutrino free-streaming wavenumber is proportional to the absolute mass scale of non-relativistic neutrino species and therefore depends on the neutrino parameters of our interest as $k_{\nu,{\rm fs}} \propto f_\nu/N_\nu^{\rm nr}$ (see [44]).

	$\Omega_{\rm m}$	$\delta_{\mathcal{R}}$	w_0	$c_{\rm e}$	f_ν	$N_\nu^{\rm nr}$	n_s	$\alpha_{\rm s}$	$\Omega_{\rm m}h^2$	$\Omega_{\rm b}h^2$	τ	$b_1(z=1)$	$b_1(z=3)$
$c_{\rm e}$	0.26	−0.02	0.18	1	0.15	−0.77	−0.05	0.03	0.23	−0.23	−0.04	−0.17	−0.18

TABLE II: The correlation coefficients between the dark energy sound speed parameter $p_{c_{\rm e}}$ (see Eq. [21]) and the other parameter p_α for the parameter error estimates for WFMOS combined with Planck. The fiducial values for dark energy parameters are set to $w_0 = -0.8$ and $c_{\rm e} = 0.05$. The sound speed is most degenerated with the non-relativistic neutrino parameter $N_\nu^{\rm nr}$.

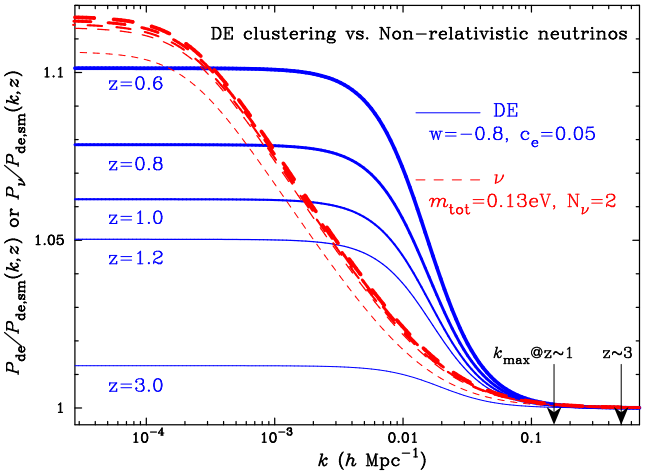

FIG. 5: Effects of the dark energy clustering (solid curves) and the massive neutrinos (dashed) on the linear power spectrum shape, relative to the smooth dark energy model. The five curves from top to bottom are the results for $z = 0.6, 0.8, 1.0, 1.2$ and 3, respectively. We assume $c_{\rm e} = 0.05$, corresponding to the jagged feature in the curve of Fig. 4, and $w_0 = -0.8$ for the dark energy fiducial model and assume $f_\nu = 0.01$ and $N_\nu^{\rm nr} = 2$ for the neutrino mass and the number of non-relativistic neutrino species. Note that the dashed curves for the neutrinos are multiplied by an arbitrary factor so that $P_\nu(k)/P_{\rm de,sm} \to 1$ at large k, taking into account the fact that the galaxy power spectrum amplitude involves uncertainty related to galaxy bias. It is clear that the redshift dependences of the two effects are quite different. The two arrows in the horizontal axis denote $k_{\rm max}$ for the $z \sim 1$ and $z \sim 3$ surveys as given in Table I.

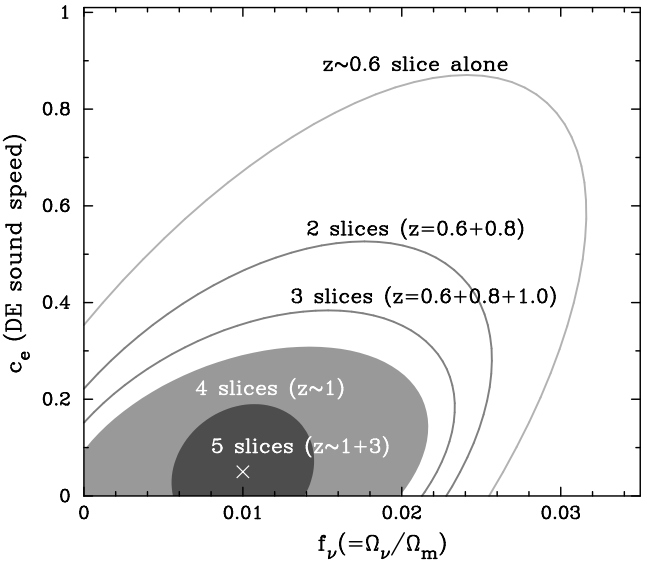

FIG. 6: Projected 68% ellipses in f_ν and $c_{\rm e}$ sub-space. The error ellipses shrink more as more redshift slices are added. In particular, for the nominal WFMOS survey, a $z \sim 3$ survey helps break the degeneracy between the two parameters efficiently, even though the slice is insensitive to dark energy. Note that the prior $\sigma(w_0) = 0.05$ is employed.

Figs. 5 and 6 give a more quantitative explanation on the results in Fig. 4. Figure 5 compares the effects of the dark energy clustering and the non-relativistic neutrinos on the linear power spectrum shape, for 5 redshift epochs. We have assumed $w_0 = -0.8$ and $c_{\rm e} = 0.05$ for the fiducial values of dark energy parameters as in Table II. It is intriguing to find the scale-dependent modifications in $P_g(k,z)$ due to these two effects are quite different: the dark energy clustering induces sharper k-transitions in $P_g(k,z)$ as well as stronger redshift dependence than the non-relativistic neutrinos do. This difference can be explained as follows. The neutrino free-streaming effect on $P_g(k,z)$ has accumulated over a longer time duration since the neutrino became non-relativistic, at $z_{\rm nr} \approx 240$ for $m_{\nu,i} \approx 0.13$ eV of our fiducial model, resulting in the modification of the linear power spectrum shape over a wider range of k. One the other hand, the dark energy clustering affects $P_g(k,z)$ only at low redshifts $z \lesssim 1$. One can thus utilize the different redshift- and k-dependences to separate the two effect from the galaxy power spectrum, if wider redshift and wavenumber coverages are available.

Fig. 6 shows the projected 68% C.L. contours in the f_ν-$c_{\rm e}$ sub-space, obtained when only one of the redshift slices for WFMOS is used or some/all of the slices are combined. Note that the prior $\sigma(w_0) = 0.05$ was employed in this plot[3]. It is clear that, as a wider redshift coverage is available, the degeneracy between f_ν and $c_{\rm e}$ determination can be more broken. It is interesting to note that adding the $z \sim 3$ slice into the $z \sim 1$ slices can further shrink the error ellipses, even though the dark energy clustering is negligible at $z \sim 3$. This is because a higher redshift survey is more powerful for constraining the neutrino parameters due to a gain in the linear fluctu-

[3] We have so far ignored the baryon acoustic peaks in $P(k)$, and including the peaks is powerful to constrain the dark energy equation of state. To take into account this, we assume the prior $\sigma(w_0) = 0.05$ taken from [13].

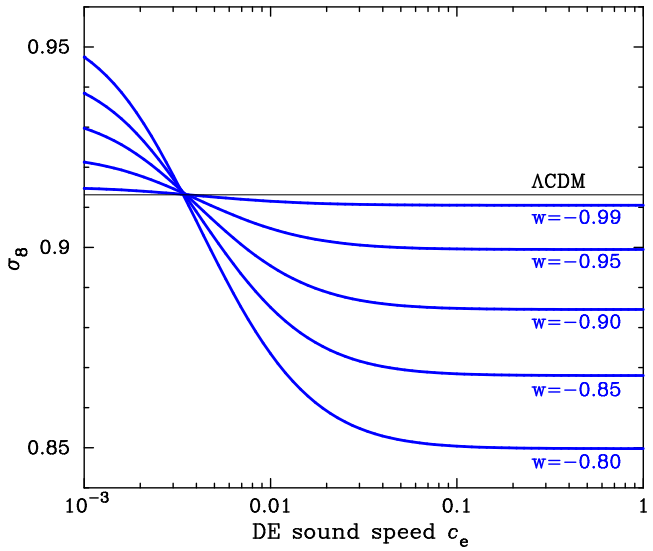

FIG. 7: Difference in σ_8 when a generalized dark energy contribution is included and the power spectrum is normalized by the primordial curvature perturbation. When $w_0 > -1$ and the sound speed is large enough, σ_8 is reduced compared to the ΛCDM prediction, because the structure formation slows down due to the more accelerated cosmic expansion at intermediate redshifts. On the other hand, when the sound speed is sufficiently small, the dark clustering enhances the power spectrum amplitude, yielding greater σ_8. The plot shows $c_e \approx 0.005$ is the critical value of c_e, where the two effects above cancel out so that the resulting σ_8 is independent of c_e and w_0, and similar to the ΛCDM prediction.

ations down to larger k (i.e. larger k_{max}), allowing a more precise measurement of the suppression in the small-scale power of $P(k)$ due to the neutrino free-streaming.

D. Effect of Dark Energy Clustering on σ_8

The cosmological parameter σ_8, the rms mass fluctuation today in spheres of radius $8h^{-1}$ Mpc, is one of the most important parameters for characterizing the clustering strength in large-scale structures at low redshifts (e.g., [55]). However, for the moment σ_8 is relatively less accurately constrained compared to the other parameters within the concordance CDM model. The three-year WMAP data alone determines σ_8 to about 7% accuracy [3]. In addition, methods based on independent data sets such as CMB, weak lensing and Ly-α data sets show slightly inconsistent best-fit values of σ_8, for example, as implied in Fig. 7 in [3] (also see [56]): the WMAP favors slightly lower σ_8 than the methods looking at the local universe.

Since the CMB observables are primarily sensitive to the perturbations at $z \sim 1000$, the present-day fluctuations, σ_8, are rather an output parameter derivable from the parameters constrained by the CMB spectra. It is becoming common to use the primordial curvature perturbation amplitude $\delta_{\mathcal{R}}$ to normalize the linear power spectra for the CMB-based methods, as we have so far employed (see Sec. IV). Then, σ_8 can be computed once the linear power spectrum shape and the growth rate from $z \sim 1000$ to present are specified to within the measurement accuracies (e.g., see [57] for a fitting formula of σ_8 for a flat CDM model with dark energy of constant equation of state). For this procedure, assuming a model with dynamical dark energy could affect an estimate of σ_8 compared to the cosmological constant model because the generalized dark energy could either suppress the growth rate due to the accelerated expansion or add the dark energy perturbation to the power of total mass perturbation. Which of these opposite two effects is dominant to determine σ_8 depends on whether the dark energy sound horizon scale is greater or smaller than $8h^{-1}$ Mpc. Hence, if a discrepancy between the σ_8 values inferred from the CMB and the local universe observations is found, it may be as a result of the dark energy contribution, and it would be worth to keep having attention to explore such a signature from the cosmological probes at different redshifts.

Fig. 7 shows how the value of σ_8 changes as a function of c_e and w_0, where other cosmological parameters are kept fixed to the fiducial values. When the sound speed c_e is large enough compared to $8h^{-1}$ Mpc, σ_8 is reduced with increasing w_0 from $w_0 = -1$ by slowing down the growth rate of mass clustering. On the other hand, if the sound speed becomes sufficiently small, albeit unrealistic, the dark energy clustering increases σ_8 as a result of adding a power to the mass clustering at scales relevant for σ_8. Another interesting result is that the critical sound speed $c_{e,cr} \approx 0.005$ emerges where the resulting σ_8 remains unchanged compared to the ΛCDM prediction.

VII. CONCLUSION AND DISCUSSION

In this paper we have investigated the ability of a future galaxy redshift survey to test the smoothness of dynamical dark energy, which is another important consequence of a generalized dark energy with $w(z) \neq -1$ and provides independent information on the nature of dark energy from that carried by the equation of state. The dark energy clustering signatures can be measured via a scale-dependent transition in the power of the galaxy power spectrum appearing at scales comparable with the dark energy sound horizon (see Fig. 1). It was shown that, for WFMOS survey, the sound speed can be detected at more than a 1-σ level, if the sound speed is small enough as $c_e \lesssim 0.04$ (0.02) when $w_0 = -0.9$ (-0.95) (see Figs. 2 and 3). An effective way to improve the ability is to enlarge the survey volume especially for low redshift slices at $z \sim 1$. An ultimate full-sky survey could improve the lower bound on the detectable c_e by a factor of 2.

Another interesting possibility of the future galaxy survey is the use of the galaxy power spectrum to weigh the neutrino mass, as investigated in [44]. We carefully in-

vestigate possible degeneracies between the dark energy clustering and the non-relativistic neutrinos in the galaxy power spectrum (see Fig. 5 and also see [58] for the related discussion on the degeneracy between the neutrino mass and the dark energy equation of state). We showed that having a wider redshift coverage can efficiently separate the two effects by utilizing the different redshift dependences; the dark energy is prominent only at low redshifts $z \lesssim 1$. In addition, modified gravity theories have received much recent attention as an alternative explanation of cosmic acceleration without dark energy, where gravity is weaker than the Einstein gravity at scales comparable to the horizon (e.g., [59, 60, 61, 62]). An important test to discriminate this possibility from the dark energy model is to simultaneously explore the cosmic expansion history and the growth of structure formation from cosmological experiments, because the two possibilities predict different growth rate even for an identical expansion history. Once again, wider redshift coverage of a galaxy redshift survey would be powerful to make a robust test of discriminating between effects of dark energy clustering, massive neutrinos, and modified gravity, which warrants a detailed study (also see [62] for the discussion on the interplay between the massive neutrinos and the modified gravity in the shape of mass power spectrum). We hope that the results shown in this paper will give a useful guidance to designing a future survey if the dark energy clustering is desired to pursue as one of the science goals.

We have assumed throughout this paper that dynamical properties of the dark energy are specified in terms of the equation of state and the effective sound speed, with the adiabatic initial condition. A merit of this approach is we need not assume a specific form of the Lagrangian of dark energy sector. However, the limitation is there is no guarantee this modeling can be applied to a full range of generic dark energy models. For example, we have ignored a contribution from the trace-free stress perturbation of dark energy, which is valid if the dark energy is a scalar field (e.g. see [25] for the extension). Since we have little idea of what dark energy is, it is worth exploring a more general modeling of dark energy properties and investigate the resulting effect on structure formation. Unless such a theoretical model is available, we cannot extract all the cosmological information inherent in the future high-precision cosmological data sets in an unbiased way.

Another non-trivial assumption we have made in this paper is the adiabatic initial conditions for dark energy perturbations, without any rigorous reasoning. If the dark energy field had existed since the inflationary epoch in the early universe, the dark energy perturbations naturally contained iso-curvature modes, and the effect just emerges at low redshifts. Hence, a galaxy redshift survey could by its own open up a new window for exploring the iso-curvature modes in structure formation to probe the physics in the early universe, complementarily to the CMB or the CMB-galaxy cross correlation [28, 30]. Furthermore, if the primordial non-Gaussianity (e.g. see [63] for a thorough review) is dominantly imprinted onto the sector of dark energy, the galaxy survey allows us to explore the signal via, e.g., the bispectrum measurement of galaxy clustering. These are our future study and will be presented elsewhere.

The linear perturbation theory makes secure predictions on structure formation, which allows an accurate interpretation of the cosmological data sets from the detailed comparison. A main obstacle that a galaxy redshift survey could contain in this procedure is uncertainties involved in the galaxy biasing, where unknown, nonlinear gastrophysics may pollute the linear information even at large scales. Although we have assumed a scale-independent, linear bias, we do not think that a more realistic bias such as a scale-dependent bias is a significant contamination to the dark energy clustering constraint. Because the dark energy clustering induces characteristic scale-dependent modification and strong redshift evolution for $P(k)$ (see Fig. 1), these properties can be very robust to discriminate the dark energy clustering signals from the galaxy bias contamination or more generally other systematics.

Finally, we comment on the non-linear gravitational clustering, which could also provide a contamination to the linear theory predictions. Encouragingly, however, the non-linear effects can be to some extent corrected based on our refined knowledge of the structure formation scenarios, based on the perturbation theory as well as the N-body simulations [61, 64, 65, 66]. Furthermore, as an interesting possibility, coupling of different Fourier modes induced by non-linear gravitational clustering could induce a transfer of the dark energy clustering effect at large scales to the power of $P(k)$ at smaller scales. If this is the case to be apparent on the measured power spectrum, an inclusion of the non-linearity in the model predictions could improve a signal-to-noise to test smoothness of dark energy, from the smaller-scale clustering information. This issue will be worth exploring in detail, and will be presented elsewhere.

Acknowledgments: The author thanks E. Komatsu for valuable discussions and also thanks for T. Futamase, O. Lahav, D. Nitta, P. Norberg and Y. Suto for helpful discussions. He also acknowledges the warm hospitality of Caltech where this work was partly done. This work was supported in part by a Grand-in-Aid for Scientific Research (17740129) of the Ministry of Education, Culture, Sports, Science and Technology in Japan as well as the COE program at Tohoku University. We acknowledge the use of the publicly-available CMBFAST code [54].

[1] S. Perlmutter et al., Astrophys. J. **517**, 565 (1999).
[2] A. G. Riess et al. Astron. J. **116**, 1009 (1998).
[3] D. Spergel et al., astro-ph/0603449.
[4] M. Tegmark et al. (The SDSS collaboration), Phys. Rev. D **69**, 103501 (2004).
[5] S. Cole et al. (The 2dFGRS Team), Mon. Not. Roy. Astr. Soc. **362**, 505 (2005).
[6] R. Scranton et al., astro-ph/0307335.
[7] D. Eisenstein et al., Astrophys. J. **633**, 560 (2005).
[8] S. Weinberg, Mod. Rev. Phys. **61**, 1 (1989).
[9] B. Ratra and P. J. E. Peebles, Phys. Rev. D **37**, 3406 (1988).
[10] P. Astier et al. (The SNLS Collaboration), A&A **447**, 31 (2006).
[11] D. Huterer, Phys. Rev. D **65**, 063001 (2002).
[12] M. Takada and B. Jain, Mon. Not. Roy. Astr. Soc. **348**, 897 (2004).
[13] H.-J. Seo and D. Eisenstein, Astrophys. J. **598**, 720 (2003).
[14] W. Hu and Z. Haiman, Phys. Rev. D **68**, 063004 (2003).
[15] T. Matsubara, Astrophys. J. **615**, 573 (2004).
[16] L. Marian and G. M. Bernstein, Phys. Rev. D in press, astro-ph/0605746 (2006).
[17] R. R. Caldwell, R. Dave and P. J. Steinhardt, Phys. Rev. Lett. **80**, 1582, (1998).
[18] T. Chiba, N. Sugiyama and T. Nakamura, Mon. Not. Roy. Astr. Soc. **301**, 72 (1998).
[19] J. Garriga and V. F. Mukhanov, Phys. Lett. B **458**, 219 (1999).
[20] R. Dave, R. R. Caldwell, and P. J. Steinhardt, Phys. Rev. D **66**, 023516 (2002).
[21] C.-P. Ma, R. R. Caldwell, P. Bode and L. Wang, Astrophys. J. Lett. **521**, 1 (1999) .
[22] W. Hu, Phys. Rev. D **65**, 023003, (2002).
[23] T. Moroi and T. Takahashi, Phys. Rev. Lett. **92**, 091301 (2004).
[24] S. Dedeo, R. Caldwell and P. Steinhardt, Phys. Rev. D **67**, 103509 (2003).
[25] J.-P. Uzan, astro-ph/0605313 (2006).
[26] R. Bean and D. Dore, Phys. Rev. D **69**, 083503 (2004).
[27] J. Weller and A. Lewis, Mon. Not. Roy. Astr. Soc. **346**, 987 (2003).
[28] C. Gordon and W. Hu, Phys. Rev. D **70**, 083003 (2004).
[29] W. Hu, Astrophys. J. **506**, 485 (1998).
[30] W. Hu and R. Scranton, Phys. Rev. D **70**, 123002 (2004).
[31] M. Kimura et al., Proceedings of the SPIE, **4841**, 974 (2003).
[32] K. Glazebrook et al., astro-ph/0507457.
[33] G. J. Hill, K. Gebhardt, E. Komatsu and P. J. MacQueen, AIP Conf. Proc., **743**, 224 (2004).
[34] G. J. Melnick et al., The NASA Origins Probe Mission Study Report, "*The Cosmic Inflation Probe: Study Report*" (2005). See also http://cfa-www.harvard.edu/cip.
[35] S. Dodelson, *Modern Cosmology*, Academic Press, San Diego, (2003).
[36] J. A. Peacock, *Cosmological Physics*, Cambridge University Press, Cambridge, (1999).
[37] J. Frieman, C. Hill, A. Stebbins and I. Waga, Phys. Rev. Lett. **75**, 2077 (1995).
[38] R. R. Caldwell, Phys. Lett.. B. **543**, 23 (2002).
[39] T. Chiba, T. Okabe and M. Yamaguchi, Phys. Rev. D **62**, 023511 (2000).
[40] C. Armendariz-Picon, V. Mukhanov and P. Steinhardt, Phys. Rev. Lett. **85**, 4438 (2000).
[41] W. Hu and D. Eisenstein, Phys. Rev. D **59**, 3509 (1999).
[42] P. J. E. Peebles, *The Large-Scale Structure of the Universe*, Princeton University Press, Princeton (1980).
[43] D. J. Heath, Mon. Not. Roy. Astr. Soc. **179**, 351 (1977).
[44] M. Takada, E. Komatsu and T. Futamase, Phys. Rev. D **73**, 083520, astro-ph/0512374 (2006).
[45] D. Eistenstein and W. Hu, Astrophys. J. **511**, 5 (1999).
[46] C. Blake and K. Glazebrook, Astrophys. J. **594**, 665 (2003).
[47] C. Alcock and B. Paczynski, Nature (London) , **281** 358 (1979).
[48] N. Kaiser, Mon. Not. Roy. Astr. Soc. **227**, 1 (1987).
[49] H. A. Feldman, N. Kaiser and J. A. Peacock, Astrophys. J. **426**, 23 (1994).
[50] M. Tegmark, A. N. Taylor and A. F. Heavens, Astrophys. J. **480**, 22 (1997).
[51] R. D. McKeown and P. Vogel, Phys. Rep. **394**, 315 (2004).
[52] O. Elgaroy, O. Lahav et al. (The 2dFRS Team), Phys. Rev. Lett. **89**, 061301 (2002).
[53] D. Eisenstein, W. Hu and M. Tegmark, Astrophys. J. **518**, 2 (1998).
[54] U. Seljak and M. Zaldarriaga, Astrophys. J. **469**, 437 (1996).
[55] N. A. Bahcall, J. P. Ostriker, S. Perlmutter and P. J. Steinhardt, Science **284**, 1481 (1999).
[56] U. Seljak, A. Slosar and P. McDonald, astro-ph/0604335.
[57] W. Hu and B. Jain, Phys. Rev. D **70**, 043009 (2004).
[58] S. Hannestad, Phys. Rev. Lett. **95**, 221301 (2005).
[59] A. Shirata, T. Shiromizu, N. Yoshida and Y. Suto, Phys. Rev. D **71**, 064030 (2005).
[60] C. Sealfon, L. Verde and R. Jimenez, Phys. Rev. D **71**, 083004 (2005).
[61] H. F. Stabenau and B. Jain, astro-ph/0604038 (2006).
[62] M. Sereno and J. A. Peacock, astro-ph/0605498 (2006).
[63] N. Bartolo, E. Komatsu, S. Matarrese and A. Riotto, Phys. Rep. **402**, 103 (2004).
[64] Y. Suto and M. Sasaki, Phys. Rev. Lett. **66**, 264 (1991).
[65] B. Jain and E. Bertschinger, Astrophys. J. **431**, 495 (1994).
[66] J. Donghui and E. Komatsu, astro-ph/0604075 (2006).